materials

MDPI

Article

Microhardness Variation with Indentation Depth for Body-Centered Cubic Steels Pertinent to Grain Size and Ferrite Content

Anye Xu, Xuding Song *, Min Ye, Yipin Wan and Chunguo Zhang

Key Laboratory of Road Construction Technology and Equipment, Ministry of Education, Chang'an University, Xi'an 710064, China; 2019225099@chd.edu.cn (A.X.); mingye@chd.edu.cn (M.Y.); wyipin@chd.edu.cn (Y.W.)
* Correspondence: songxd@chd.edu.cn

Abstract: For a micro-indentation hardness test with non-destructivity, the Nix–Gao model is widely used to describe tested hardness or microhardness variation with an indentation depth induced by indentation size effect, in which tested hardness approaches the macrohardness when the indentation depth is large enough. Based on an analysis of hardness measurements on 10 body-centered cubic steels with diverse microstructure, this paper proposes an analytical relation between microhardness to macrohardness ratio and the indentation depth by explicitly linking characteristic indentation depth (a data-fitting parameter) to grain size and ferrite volume fraction using two different methods. In addition, the normal distribution theory is incorporated to consider the inevitable scatter of identical measurements resulting from material heterogeneity and machining/testing errors. Results show that the proposed model, with 96% reliability, can effectively predict microhardness variation with the indentation depth and its scatter.

Keywords: indentation size effect; grain size; ferrite volume fraction; normal distribution

Citation: Xu, A.; Song, X.; Ye, M.; Wan, Y.; Zhang, C. Microhardness Variation with Indentation Depth for Body-Centered Cubic Steels Pertinent to Grain Size and Ferrite Content. *Materials* **2024**, *17*, 2371. https://doi.org/10.3390/ma17102371

Academic Editor: Alexander Yu Churyumov

Received: 14 April 2024
Revised: 9 May 2024
Accepted: 13 May 2024
Published: 15 May 2024

1. Introduction

The hardness of a material as a mechanical constant should be independent of loading conditions. For micro- and nano-hardness measurements, however, the tested hardness value (H) varies with the indentation depth (h) due to indentation size effect (ISE) [1,2]. In general, H decreases with increasing h, and gradually tends to a steady-state value which is regarded as material constant or macrohardness (H_0).

From the perspective of physics, the tested H value arises from the geometrically necessary dislocation (GND) and the statistically stored dislocation (SSD) of a material [3,4]. For the indentation test, strain gradient and corresponding GND increase with the decreasing indentation size [5,6]. That is why the tested H value continuously increases with the decreasing h value. For this reason, Nix and Gao developed strain gradient plasticity theory and proposed the below relation between H/H_0 and h to describe the ISE phenomenon by considering the GND mechanism [7]:

$$H = H_0\sqrt{1 + \frac{h^*}{h}} \tag{1}$$

where the characteristic indentation depth (h^*) can be obtained by data fitting.

Numerous studies were performed to study the factors related to ISE, e.g., microstructure of a material [8,9] and indenter geometry [10,11]. For instance, average grain size (G) and grain boundary significantly influence H value when h is comparable to G in size [8,12], and the length of GND and h^* values are related to G [9]. However, the quantitative relationship between h^* and G has not been determined. Chicot finds $H_0 \cdot \sqrt{h^*}$ is proportional to $\mu \cdot \sqrt{b}$ (μ is shear modulus, and b is Burgers vector), which indicates the h^* value depends on the microstructure of a material [13]. Indenter geometry also has influences on the variation

of the H–h curve, and a larger angle and bunting tip of an indenter result in slower H variation with h [14,15]. Based on the above, μ and b of a material and indenter angle are incorporated into the formula of h^* to modify the Nix–Gao model [10]. While the limitation of the existing model needs to be fitted based on experimental data.

Body-centered cubic (BCC) steels with a matrix of α-Fe are widely used in industrial applications [16]. The material hardness of a BCC steel is also influenced by ferrite volume fraction (V_F) [17]. An existing study finds that V_F influencing the h^* value is inversely proportional to dislocation density [18], and SSD density is related to dislocation mean free path (L). For a material with V_F = 100%, L value approximates G in size [18,19]. That is, G and V_F are two significant factors related to h^* value and ISE phenomenon.

In summary, h^* in the Nix–Gao model is a data-fitting parameter which lacks a clear physical meaning. Based on the above discussions and in order to predict macrohardness H_0, it is reasonable to link h^* with G and V_F for BCC steels to determine an analytical description of the widely used Nix–Gao model. As illustrated in Figure 1, the intersection of two asymptotic curves is h^*, indicating the translation from infinite hardness to H_0. In the field of non-linear elastic fracture mechanics, the characteristic crack size (a^*_{ch}) indicates the transition from tensile strength-controlled to fracture toughness-controlled for the fracturing of brittle materials [20]. Interestingly, we find that a non-linear elastic fracture model and the Nix–Gao model are similar in form, and the characteristic parameter a^*_{ch} is similar to h^*. Our previous studies quantitatively link a^*_{ch} with G for ceramics and obtain a quantitative relation of $a^*_{ch} = \pi \cdot G$ through the analysis of experimental data [21]. Inspired by this, two methodologies: (i) theoretical derivation and (ii) the analysis of experimental data are adopted in this study to propose an analytical H_0/H–h relation by explicitly linking h^* to G and V_F based on the Nix–Gao model by analyzing Vickers hardness measurements on 10 BCC steels (G = 10.00–34.41 μm and V_F = 5–100%). Additionally, the normal distribution theory is incorporated into the model to consider the inevitable scatter in material properties resulting from material heterogeneity and machining/testing errors [22,23].

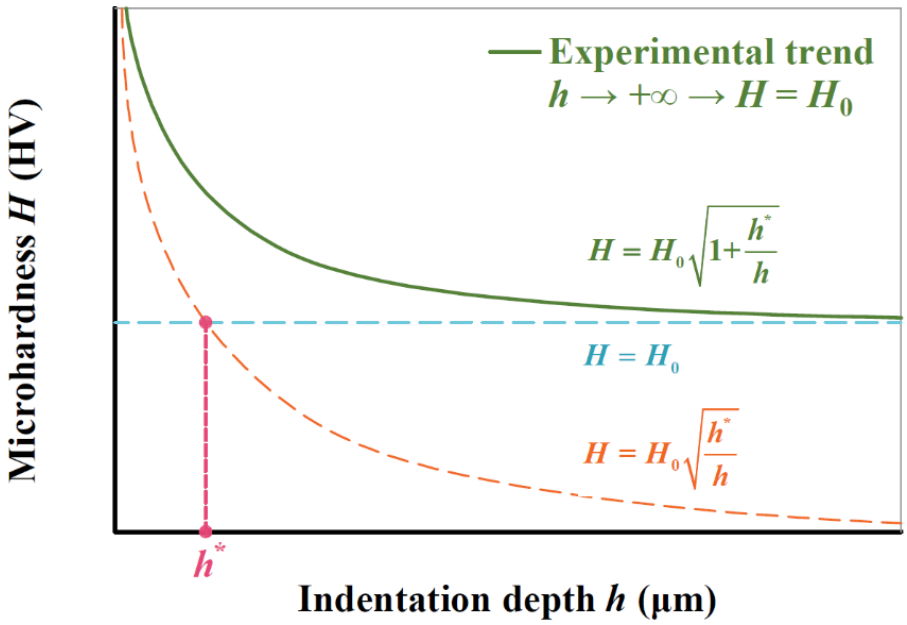

Figure 1. Nix–Gao model showing H variation with h.

2. Experiments and Data

2.1. Measurements on Hardness, Grain Size and Ferrite Volume Fraction

Four BCC steels in Table 1: Q345B, 20 steel, and 45 steel from BaoWu Steel, Shanghai, China, and ER50-G from Golden Bridge Welding Materials, Tianjin are measured in this study. The microstructure of the steels is examined using an optical microscope after

polishing and etching with 4% nital solution (4 mL HNO_3 and 96 mL alcohol). Vickers hardness is measured by using a Wilson 402 MVD Vickers (Chang'an University, Xi'an, China) hardness tester with different loads (10 g, 25 g, 50 g, 100 g, 200 g, 300 g, 500 g, and 1 kg) with a dwell time of 20 s, and five measurements are performed under each load to get reliable results. According to ASTM E92 [24], the applying load (P) should be greater than 5 kg for H_0 measurements. Thus, 10 kg is adopted to obtain H_0 using a HV-10 Vickers hardness tester.

Table 1. Chemical compositions of materials tested in this study (in wt. %).

Materials	C	Si	Mn	P	S	Cu	Cr	Ni	Fe
Q345B	0.14	0.5	1.7	0.035	0.035	0.30	0.3	0.05	Balance *
ER50-G	0.07	0.9	1.5	0.012	0.011	0.5	0.02	0.02	Balance
20 steel	0.2	0.22	0.53	0.035	0.035	0.07	0.04	0.01	Balance
45 steel	0.45	0.17	0.5	0.035	0.035	0.25	0.25	0.25	Balance

* Balance: The proportion of elements other than those already listed.

Based on the microstructure image, G is measured using the intercept method according to ASTM E112 [25] (Figure 2a). V_F is obtained using the method shown in Figure 2b: an optical microstructure picture with two phases is converted to a black–white photo (white area indicates ferrite), and the proportion of the white area is V_F [19].

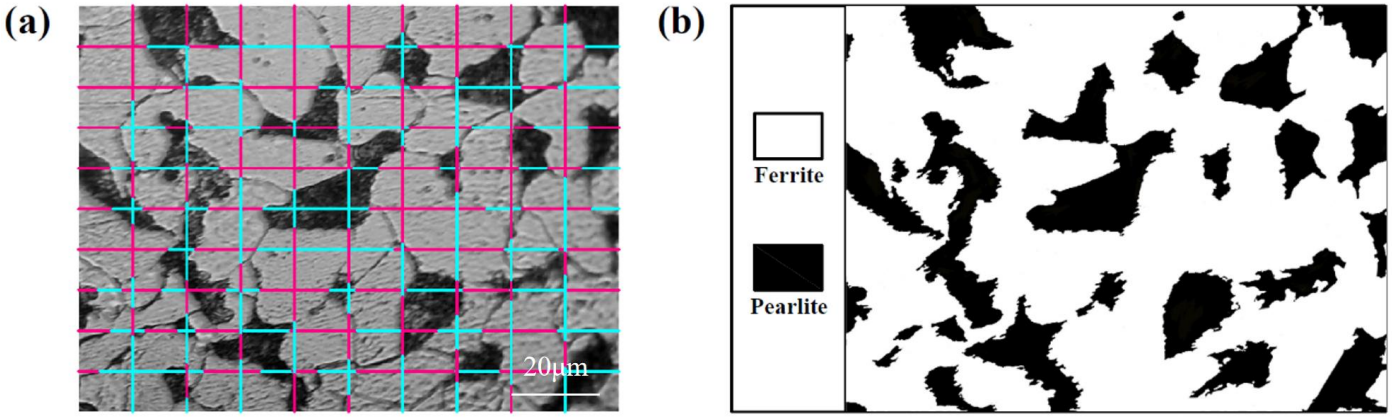

Figure 2. Illustrations of measuring (**a**) average grain size G and (**b**) ferrite volume fraction V_F for 20 steel.

2.2. Experimental Data

Figure 3 shows the observed microstructure and H variation with h value for Q345B, ER50-G, 20 steel and 45 steel. The microstructure, V_F, G and H_0 of the four steels are listed in Table 2 together with those of other six BCC steels in the literature. It should be mentioned that only the maximum, minimum and mean values under each load are digitized for the hardness data (h, H) on the six BCC steels. The 10 BCC steels consist of up to two metallurgical structures (one of them is ferrite), in which Grade 91 10A and 10B steels consist mainly of martensite and a little ferrite [26,27], the high carbon steel with 0.71% C consists of spheroids cementite and ferrite [28], and the other seven steels consist of pearlite and ferrite.

Table 2. Material parameters of BCC steels used in this study [12,26,28–31].

Materials	Phase	V_F	G (μm)	H_0 (HV)
Q345B	F * + P *	84%	8.17	171.9
ER50-G	F + P	94%	5.19	218.2
20 steel	F + P	76%	14.14	156.6

Table 2. *Cont.*

Materials	Phase	V_F	G (μm)	H_0 (HV)
45 steel	F + P	43%	10.01	199.5
IF steel [12]	F	100% [28]	24.29 [12]	94.5 [12]
Low carbon steel (0.19% C) [12]	F + P	72% [28]	34.41 [12]	206.7 [12]
Medium carbon steel (0.32% C) [12]	F + P	58% [28]	19.23 [12]	237.0 [12]
High carbon steel (0.71% C) [12]	F + SC *	56%	16.43 [12]	244.1 [12]
Grade 91 10A steel [29]	F + M *	5% [26]	30.00 [30]	164.7 [29]
Grade 91 10B steel [29]	F + M	5% [26]	10.00 [31]	240.0 [29]

* Ferrite (F), pearlite (P), spheroidal cementite (SC), and martensite (M).

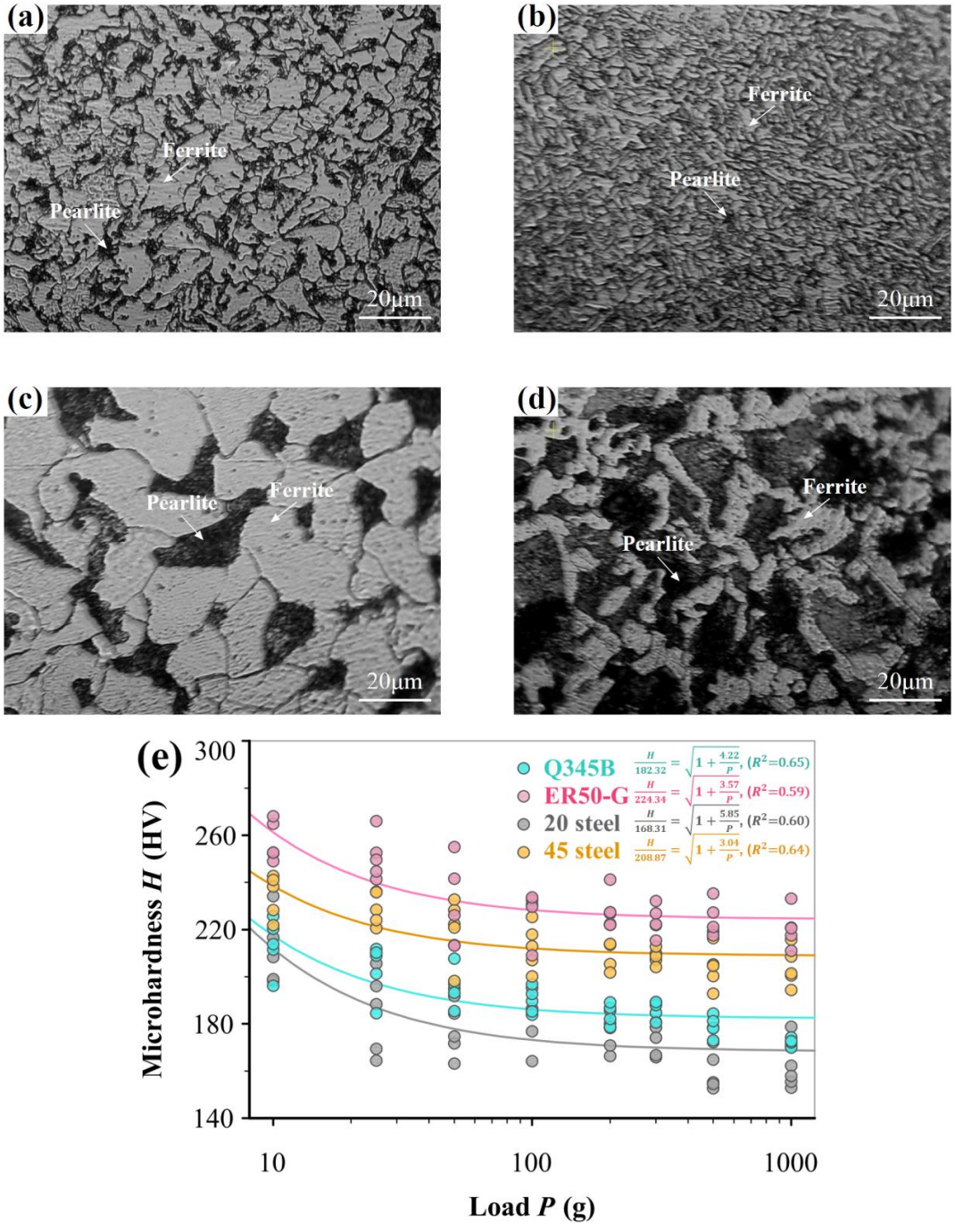

Figure 3. Microstructure of (**a**) Q345B, (**b**) ER50-G, (**c**) 20 steel and (**d**) 45 steel, and (**e**) Vickers microhardness variation with applying load.

3. Analytical H–H_0 Relation by Linking h^* to G and V_F

To ensure the reliability, the analytical formula describing H/H_0 variation with h is proposed based on two different methodologies (theoretical derivation and statistical analysis of experimental data) as shown in Sections 3.1 and 3.2, respectively. In Section 3.3, the normal distribution analysis is incorporated in the formula to describe the inevitable scatter of measurements under identical conditions.

3.1. Theoretical Derivation

The ISE phenomenon during micro- and nano-hardness measurements can be formulated as Equation (1). Recent studies find that h^* is related to microstructure, material properties and indenter geometry as follows [10]:

$$h^* = \frac{81}{2}\frac{1}{f^3}\alpha^2 b \tan^2\theta\left(\frac{\mu}{H_0}\right)^2 \tag{2}$$

where the scaling factor $f = a_{PDZ}/a \approx 1.9$ (a_{PDZ} is the plastic zone size after indenting and a is indentation radius) for steels [32], indenter geometry parameter $\theta = 22^\circ$ for Vickers indenter, and $\alpha \approx 0.5$, Burgers vector $b \approx 0.248$ nm and shear modulus $\mu \approx 80$ GPa for BCC steels [12].

Yield strength σ_y of a material includes two parts [33] as follows:

$$\sigma_y = \sigma_{GB} + \sigma_0 \tag{3}$$

where σ_{GB} is the contribution of grain boundaries to strength, and σ_0 includes precipitation strengthening and solid solution strengthening. In the Hall–Petch relation, σ_{GB} is a function of average grain size G [34], as follows:

$$\sigma_{GB} = k_y G^{-0.5} \tag{4}$$

where the Hall–Petch coefficient k_y can be obtained by data fitting or the following formula [35]:

$$k_y = \beta\mu\sqrt{b} \tag{5}$$

where β is a dimensionless data-fitting parameter. The parameter $k_y \approx 20$ MPa$\sqrt{\text{mm}}$ is for steels [36], thus $\beta \approx 0.5$ is calculated based on Equation (5). In numerical terms, the contribution of grain boundaries to hardness (H_{GB}) can be linked to σ_{GB} [34,36,37] as follows:

$$H_{GB} = 3\sigma_{GB} = 3\beta\mu\sqrt{b}G^{-0.5} \tag{6}$$

It is easy to understand that the hardness of a material is pertinent to both metallography organization and grain size. For materials with ferrite, V_F has significant influence on the mechanical properties (e.g., hardness, yield strength, and plastic deformation). To consider both G and V_F influences, and inspired by the Hall–Patch relation, a concept of relative grain size (G_r) is introduced in this study:

$$G_r = G{\cdot}e^{(V_F-1)} \tag{7}$$

Thus, the following equation can be obtained by replacing G in Equation (6) by G_r:

$$H_{GB} = 3\beta\mu\sqrt{b}(G_r)^{-0.5} = 3\beta\mu\sqrt{b}\left(G{\cdot}e^{(V_F-1)}\right)^{-0.5} \tag{8}$$

Similarly, Equation (2) can be rewritten as below by replacing H_0 by H_{GB}:

$$h^* = \frac{81}{2}\frac{1}{f^3}\alpha^2 b\ \tan^2\ \theta\left(\frac{\mu}{3\beta\mu\sqrt{b}\left(G{\cdot}e^{(V_F-1)}\right)^{-0.5}}\right)^2 = \frac{81\alpha^2\ \tan^2\ \theta}{18f^3\beta^2}{\cdot}G{\cdot}e^{(V_F-1)} \tag{9}$$

For BCC steels with α-Fe as matrix, f, θ, and α in Equation (2) and β in Equation (5) are specific, thus $h^* = 0.107 \approx 0.1G{\cdot}e^{(VF-1)}$. Then, Equation (1) can be rewritten as follows:

$$H = H_0\sqrt{1 + \frac{0.1G{\cdot}e^{(V_F-1)}}{h}} \tag{10}$$

3.2. Analysis of Experimental Data

Based on Taylor's dislocation model and von Mises rule, tested hardness H resulted from GND and SSD, can be quantified as below [3]:

$$H = 3\sqrt{3}\alpha\mu b\sqrt{\rho_G + \rho_S} \tag{11}$$

where ρ_G is GND density and ρ_S is SSD density.

In Equation (11), ρ_G is a function of h [3].

$$\rho_G = \frac{3}{2bh}\tan^2\theta \tag{12}$$

When h is infinite or large enough, ρ_G goes to zero, and H can be regarded as H_0. That is, H_0 is only governed by SSD, and Equation (11) can be rewritten as follows:

$$H_0 = 3\sqrt{3}\alpha\mu b\sqrt{\rho_S} \tag{13}$$

In Equation (13), ρ_S can be linked to microstructure [18].

$$\rho_S = \frac{1}{c^* bL}(1 - e^{-3c^*\varepsilon^*}) \tag{14}$$

where L is dislocation mean free path, and the representative strain $\varepsilon^* = 0.2\cdot\tan\theta = 0.08$ for Vickers indentation tests [18,38], and c^* can be obtained by data fitting. For a steel with $V_F = 100\%$, $L \approx G$ [19], and the maximum value of L in a steel with $V_F < 100\%$ is not more than G value [39]. Based on the above discussion, it can be concluded that the L value is closely related to both G and V_F for BCC steels. Inspired by this, the following relation is assumed:

$$L = G\cdot e^{(V_F - 1)} \tag{15}$$

Combining Equations (11)–(15), the following equation is obtained:

$$\frac{H}{H_0} = \sqrt{\frac{\rho_S + \rho_G}{\rho_S}} = \sqrt{1 + \frac{\frac{3}{2bh}\tan^2\theta}{\frac{1 - e^{-3c^*\varepsilon^*}}{c^* bG\cdot e^{(V_F - 1)}}}} = \sqrt{1 + \frac{C\cdot G\cdot e^{(V_F - 1)}}{h}} \tag{16}$$

where $C = 1.5c^*\tan^2\theta/(1 - e^{-0.6c^*\tan\theta})$.

Comparing Equation (16) with Equation (1), $h^* = CG\cdot e^{(VF - 1)}$. The difference is that parameter h^* in Equation (1) is a data-fitting parameter, and $CG\cdot e^{(VF - 1)}$ in Equation (16) has an explicitly physical meaning if C is specific.

As we all know, microhardness measurements on the same material under identical conditions inevitably fluctuate due to material heterogeneity and testing/machining errors. In Equation (16), G and V_F are specific for a material, and H and h can be directly obtained for an experiment. Thus, H_0 value can be calculated using Equation (16) if C is a constant. It is easy to understand that H_0 values should follow normal distribution for a group of measurements on a material. If the C value varies, the corresponding mean and stand deviation values will change for the same group of measurements. From a mathematic point of view, it is reasonable that a minimum of standard deviation (σ_{H0}) exists with C variation when C becomes a critical value C_0 as illustrated in Figure 4a.

To determine the specific value of C, measurements on low carbon steel (0.19% C), high carbon steel (0.71% C) and Grade 91 10A steel in the literature are analyzed together with measurements on Q345B steel in this study in Figure 4. The corresponding material parameters are listed in Table 2.

Clearly, the standard deviation of H_0 (σ_{H0}) varies continuously with the C value, and a critical value C_0 exists, which corresponds to the minimum of σ_{H0}. It can be seen that the C_0 value varies from 0.097 to 0.123, and the average of the C_0 values approximates 0.109.

Figure 5 shows coefficient of variation (CV = standard-deviation/mean) variation with the C value for the same data in Figure 4, which describes the relative scatter of data. Similarly, CV of H_0 varies continuously with the C value, and a critical value C_0 exists,

which corresponds to the minimum of CV of H_0. C_0 value varies from 0.094 to 0.112 can be seen, and the average of the C_0 values approximates 0.104.

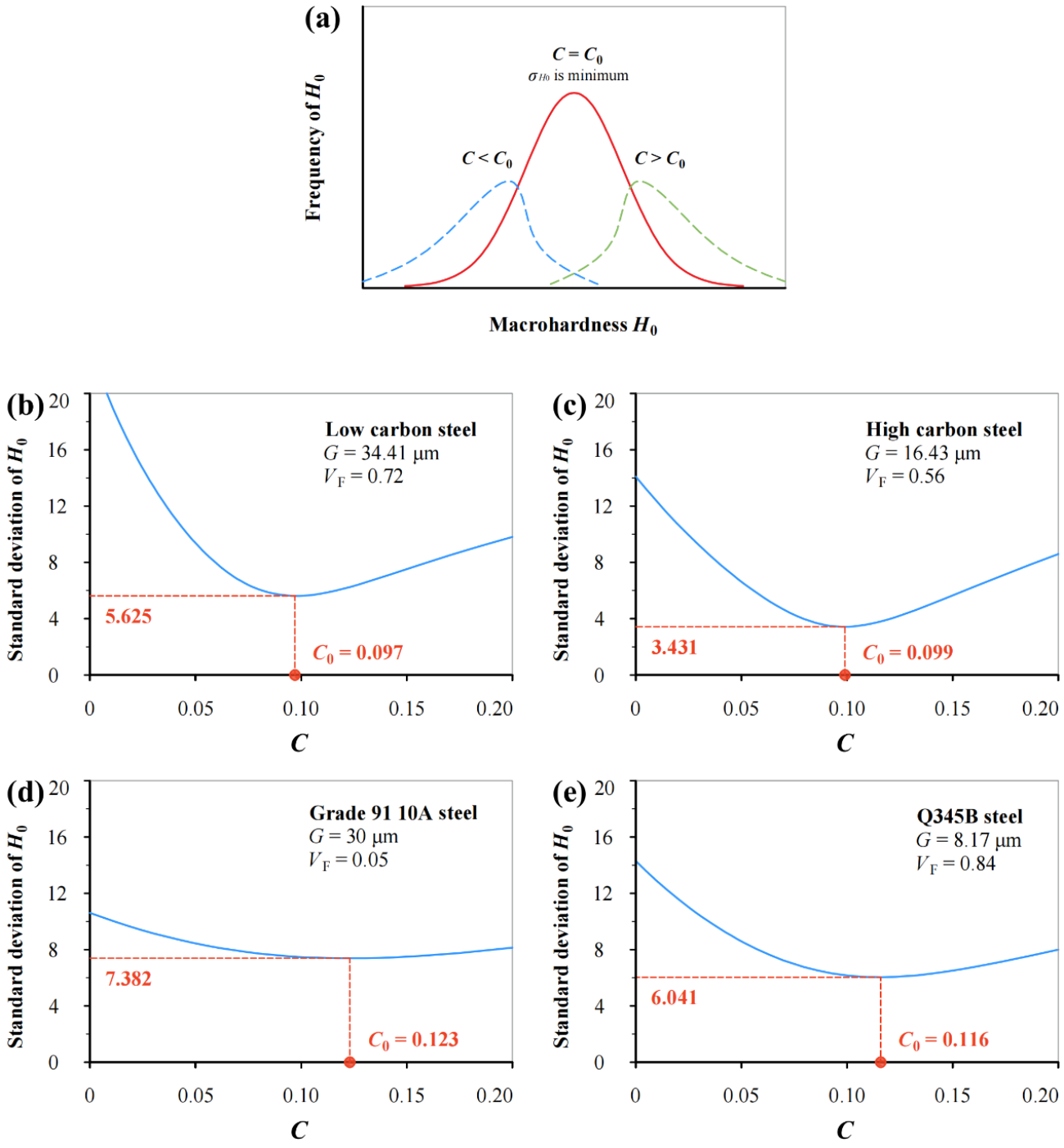

Figure 4. (**a**) Illustration of H_0 variation with C value based on Equation (16) for (**b**) low carbon steel (0.19% C), (**c**) high carbon steel (0.71% C), (**d**) Grade 91 10A steel, and (**e**) Q345B steel.

Figure 6 shows the variation in range of $(H_0)_{max}$–$(H_0)_{min}$ with the C value for the same data in Figure 4. Again, the minimum of $(H_0)_{max}$–$(H_0)_{min}$ occurs when C becomes a critical value C_0. The variation in the C_0 value from 0.071 to 0.104 can be seen, and the average of the C_0 values approximates 0.092.

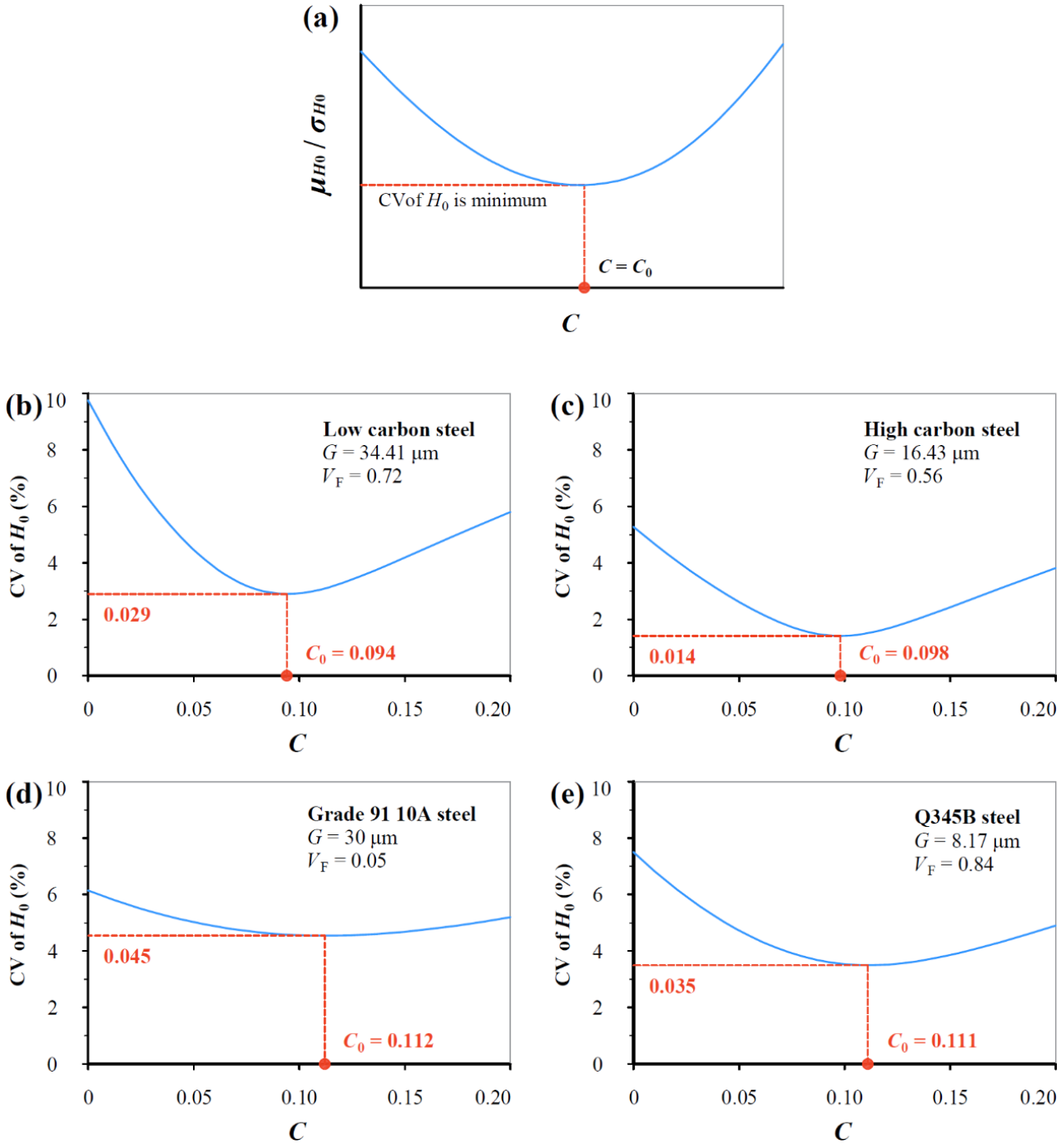

Figure 5. (**a**) Illustrating the CV variation with *C* value based on Equation (16) for (**b**) low carbon steel (0.19% C), (**c**) high carbon steel (0.71% C), (**d**) Grade 91 10A steel, and (**e**) Q345B steel.

According to the above analyses, adopting three different mathematical statistical methods for the same measurements (four groups in total), it is found that the critical value C_0 fluctuates around 0.1. For simplicity and consistency, it is reasonable to set C_0 = 0.1 in this study. Thus, H/H_0 variation is successfully described as linked to both *G* and V_F, i.e., $h^* = 0.1G \cdot e^{(VF-1)}$. That is, Equation (16) can be rewritten as Equation (10). It should be mentioned that the same equation can be obtained by using different methodologies in Sections 3.1 and 3.2.

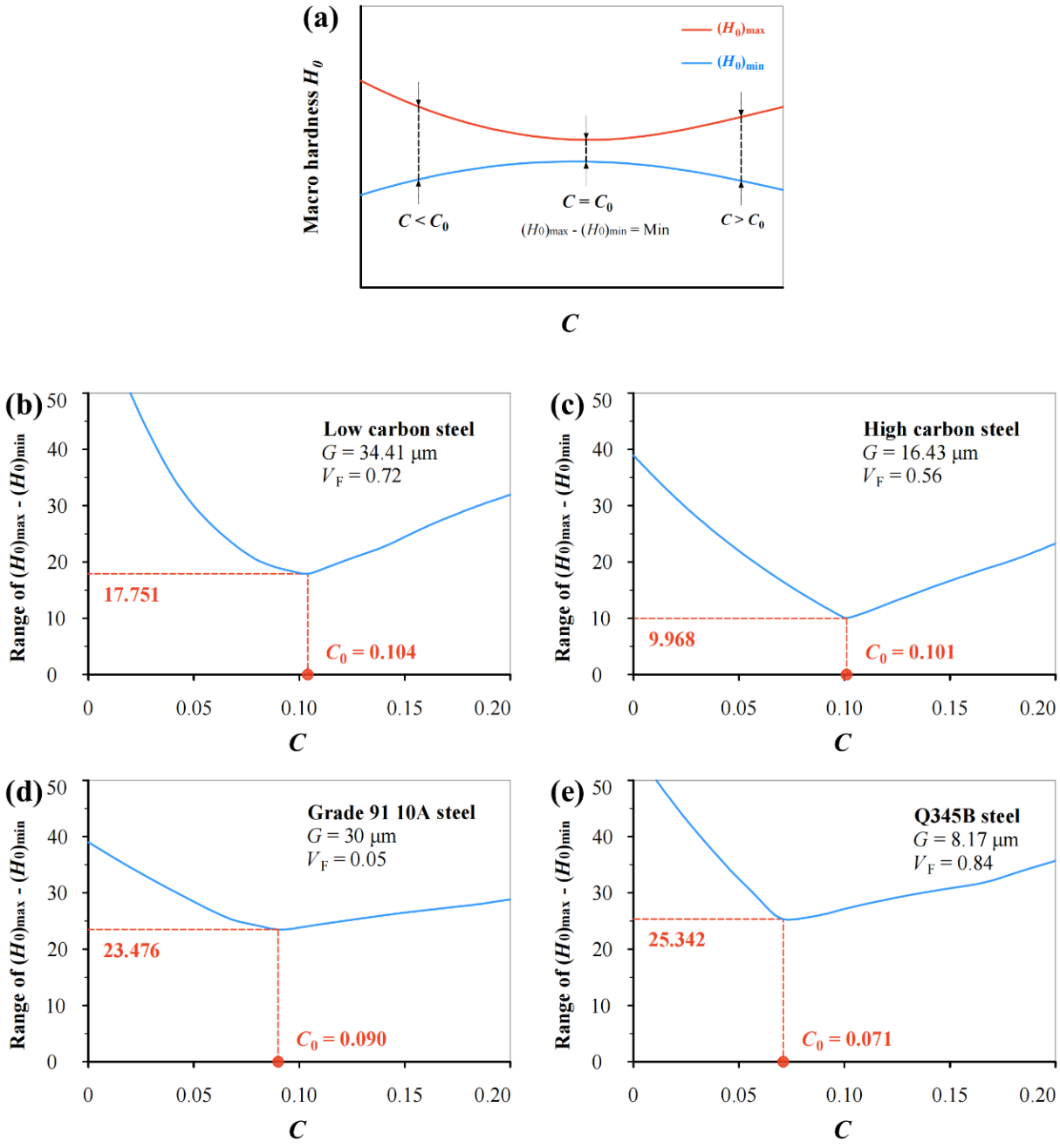

Figure 6. (**a**) Illustrating the variation in range of $(H_0)_{max}$–$(H_0)_{min}$ with C value based on Equation (16) for (**b**) low carbon steel (0.19% C), (**c**) high carbon steel (0.71% C), (**d**) Grade 91 10A steel, and (**e**) Q345B steel.

3.3. Normal Distribution Analysis for Inevitable Scatter of H/H_0

In theory, the right side of Equation (10) is constant for a material under the same loading conditions, but the tested values of H on the left side inevitably fluctuate because of material heterogeneity and testing/matching errors. For this reason, a non-dimensional parameter λ is incorporated into Equation (10):

$$\frac{H}{H_0} = \lambda \cdot \sqrt{1 + \frac{0.1G \cdot e^{(V_F - 1)}}{h}} = \lambda \cdot f(h, G, V_F) \quad (17)$$

Obviously, the H/H_0 ratio is fully determined by G, V_F, and h. For a group of tested H values, corresponding λ values, calculated using Equation (17), can be analyzed

using the normal distribution theory to obtain mean μ_λ and standard deviation σ_λ. Thus, Equation (17) can be re-reformulated to include both mean, and upper and lower bounds with 96% reliability:

$$\frac{H}{H_0} = (\mu_\lambda \pm 2\sigma_\lambda)\cdot\sqrt{1+\frac{0.1G\cdot e^{(V_F-1)}}{h}} = (\mu_\lambda \pm 2\sigma_\lambda)\cdot f(h, G, V_F) \quad (18)$$

To determine the values of μ_λ and σ_λ, the four groups of data in Figure 4 are reanalyzed in Figures 7 and 8. It can be seen from Figure 7 that μ_λ fluctuates from 0.933 to 1.106 and σ_λ from 0.014 to 0.045. Figure 8 shows the predicted H/H_0–$f(h, G, V_F)$ curves using Equation (18) in linearity using the μ_λ and σ_λ values in Figure 7 together with fitted curves for comparison, in which the $\mu_\lambda \pm 2\sigma_\lambda$ values indicate the slopes of three predicted lines. It can be seen that the experimental points are almost covered by the predicted curves, in which the mean curves are nearly identical to fitted curves.

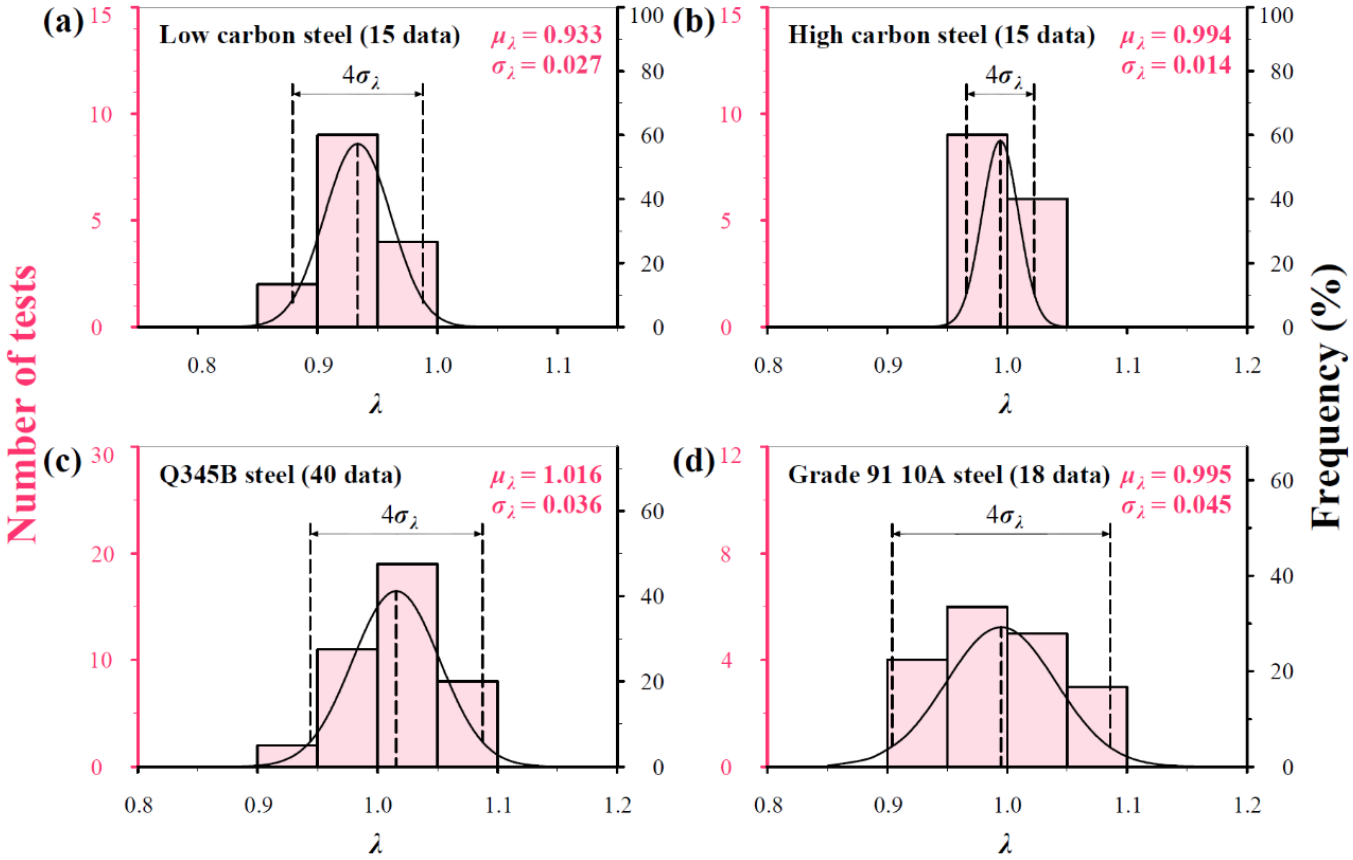

Figure 7. Histograms and frequencies of λ distributions from measurements on (**a**) low carbon steel (0.19% C), (**b**) high carbon steel (0.71% C), (**c**) Q345B steel, and (**d**) Grade 91 10A steel.

Although μ_λ fluctuates from 0.933 to 1.106 for the four measurements, it should be 1.0 in theory. Considering the limitation of small sample data, the σ_λ value should be no less than the maximum of 0.045 in Figure 7. For consistency, the rule of μ_λ = 1.0 and σ_λ = 0.05 is set in this study, thus Equation (18) can be rewritten as follows:

$$\frac{H}{H_0} = (1.0 \pm 2\times 0.05)\cdot\sqrt{1+\frac{0.1G\cdot e^{(V_F-1)}}{h}} = (1.0 \pm 2\times 0.05)\cdot f(h, G, V_F) \quad (19)$$

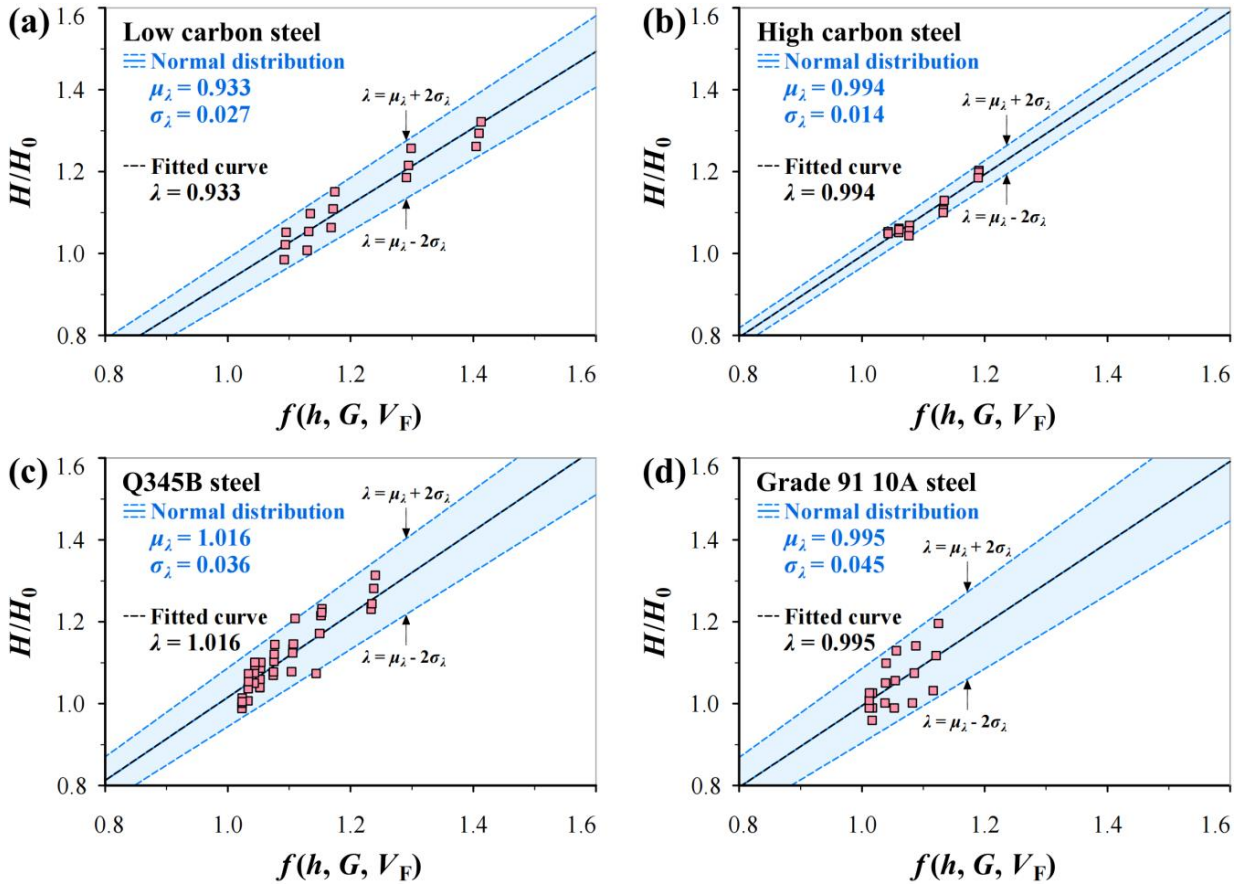

Figure 8. Predicted H/H_0–$f(h, G, V_F)$ relations using Equation (18) in linearity using μ_λ and σ_λ values in Figure 7 together with fitted curves: (**a**) low carbon steel (0.19% C), (**b**) high carbon steel (0.71% C), (**c**) Q345B steel, and (**d**) Grade 91 10A steel.

4. Verification

To validate Equation (19), hardness measurements on six BCC steels in Table 2 are used: IF steel, medium carbon steel (0.32% C) and Grade 91 10B steel in the literature, and ER50-G, 20 steel and 45 steel in this study. Figure 9 shows the predicted H/H_0–h curves using Equation (19) together with fitted curves and test data for comparison. It can be seen that the predicted curves with mean and upper and lower bounds cover most of the experimental data points.

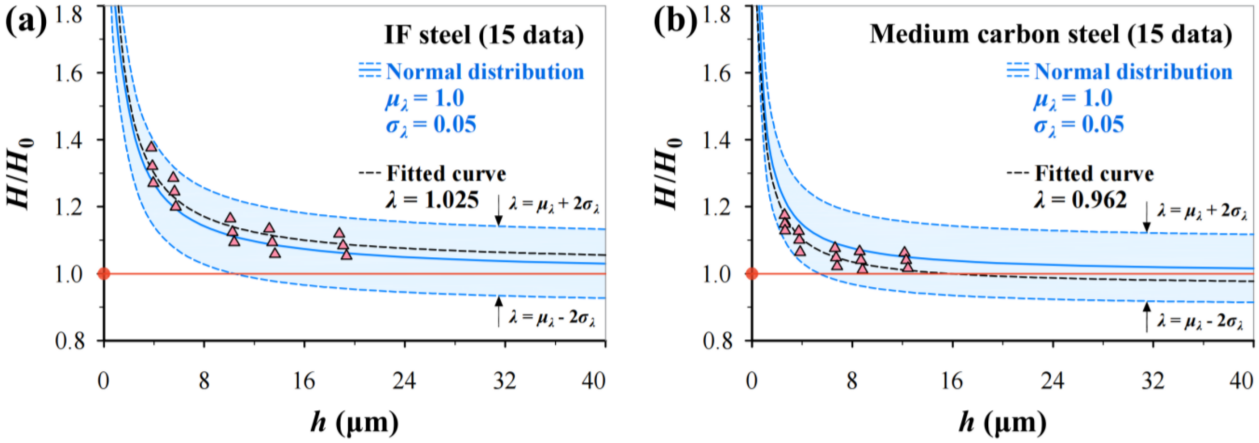

Figure 9. *Cont.*

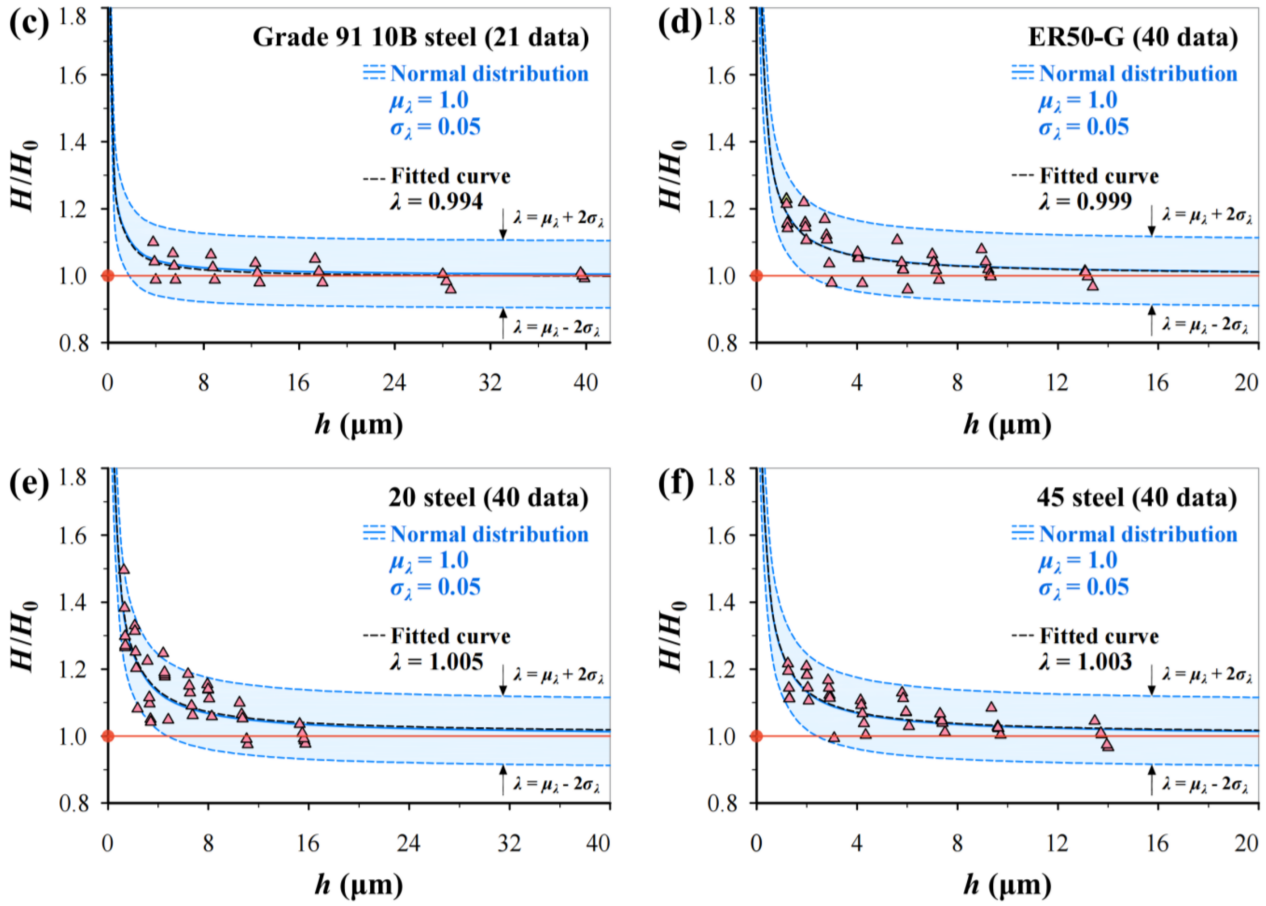

Figure 9. Predicted H/H_0–h relations using Equation (19) together with fitted curves and experimental data: (**a**) IF steel, (**b**) medium carbon steel (0.32% C), (**c**) Grade 91 10B steel, (**d**) ER50-G, (**e**) 20 steel, and (**f**) 45 steel. The red line indicates a trend line.

Figure 10 shows the predicted H/H_0–$f(h, G, V_F)$ curves using Equation (19) in linearity without changing accuracy, in which $1.0 \pm 2 \times 0.05$ indicates the slopes of three predicted lines. It can be seen that the predicted mean curves are very close to the corresponding fitted curves.

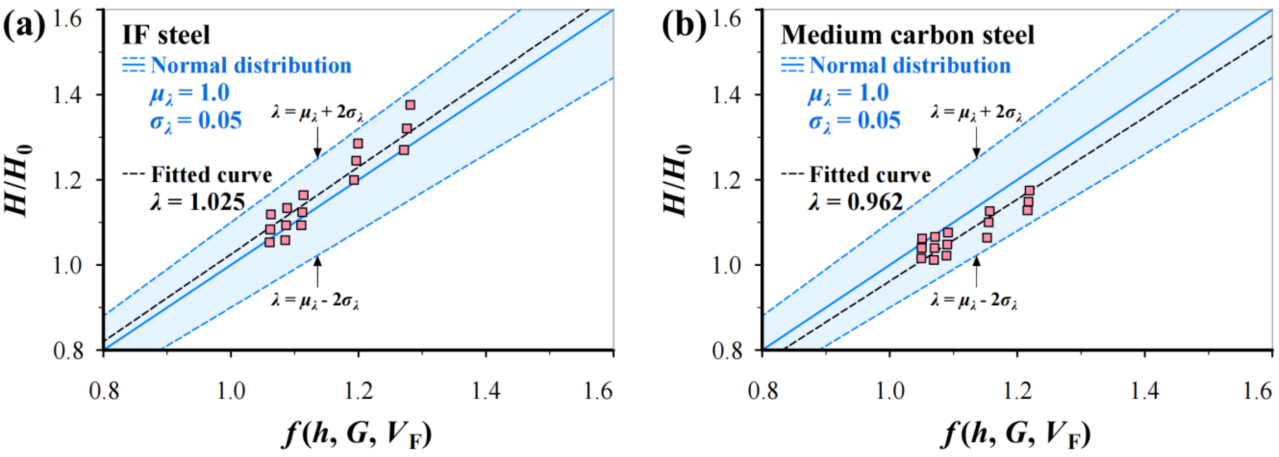

Figure 10. *Cont.*

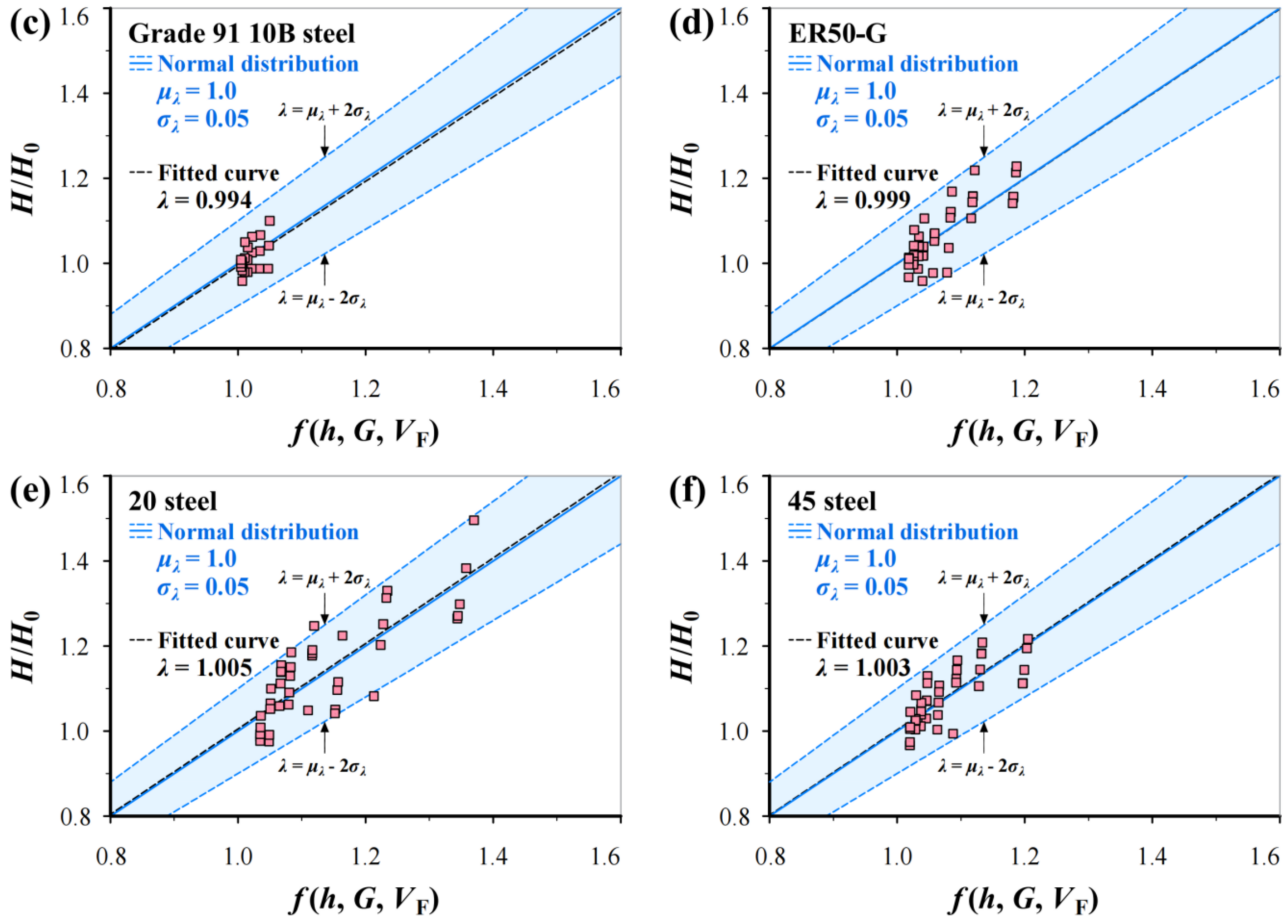

Figure 10. Predicted H/H_0–$f(h, G, V_F)$ relations using Equation (19) in linearity together with fitted curves and experimental data: (**a**) IF steel, (**b**) medium carbon steel (0.32% C), (**c**) Grade 91 10B steel, (**d**) ER50-G, (**e**) 20 steel, and (**f**) 45 steel.

5. Discussion

For the micro-indentation hardness test, the ISE phenomenon cannot be ignored. The widely used Nix–Gao model can describe the microhardness variation; however, the empirical parameter h^* leads to a limitation of application for testing the material constant. Numerous studies show that tested H is not only related to the h value, but also related to the microstructure and phase content of a material. To investigate the hardness characteristics for BCC steels, which are widely used in industrial applications, h^* is explicitly linked to G and V_F ($h^* = 0.1G{\cdot}e^{(VF-1)}$) by two different methods to consider the grain size and phase content. The proposed model can be used to calculate the hardness of a material H_0 based on tested data (h, H). Moreover, shallow indentation or low h value has no influence on the calculation accuracy of H_0 but can significantly reduce the surface damage of materials or components. Thus, H_0 can be easily obtained in microhardness tests with small load.

For BCC steels, larger G and higher V_F result in lower dislocation density leading to lower strength and higher plastic deformation capacity. Figure 9 shows that the H/H_0–ratio with increasing h more easily approaches the steady state of one for Grade 91 10B steel than other steels. This is because Grade 91 10B has a mainly martensite structure, and V_F is lower than other materials, which results in a higher dislocation density. In fact, complex microstructural features such as secondary phases and carbide precipitation significantly affect test results. Thus, the influence of more factors on microhardness variation can be reflected by H. That is why only G and V_F are considered part of h^* of the Nix–Gao model and good robustness for different BCC steels can be found.

The scatter of hardness measurements under the same loading condition is inevitable due to the micro-heterogeneity of a material, and it increases with decreasing h. Therefore, normal distribution analysis is incorporated into the proposed model. To further validate Equation (19), Figure 11 shows the integrated analysis of measurements on 10 BCC steels. The q-q plot (Figure 11a) of λ values from all 259 data proves that the measurements on different materials still obeys normal distribution, as the correlation coefficient R = 0.998, and the unified normal distribution parameters (μ_λ = 1.0 and σ_λ = 0.05) are deemed acceptable by comparing the predicted curves with the histogram from measurements. Clearly, the prediction using Equation (19) agrees well with the experimental data, and the predicted curves with upper and lower bounds (96% reliability) cover most of the experimental points. Equation (19) can be flexibly used in linearity and non-linearity, as shown in Figure 11c,d. In addition, Figure 11d shows that the H/H_0 ratio is less than 1.025 when $h/[G{\cdot}e^{(VF-1)}] > 5$, in which the tested value H can be regarded as material hardness H_0.

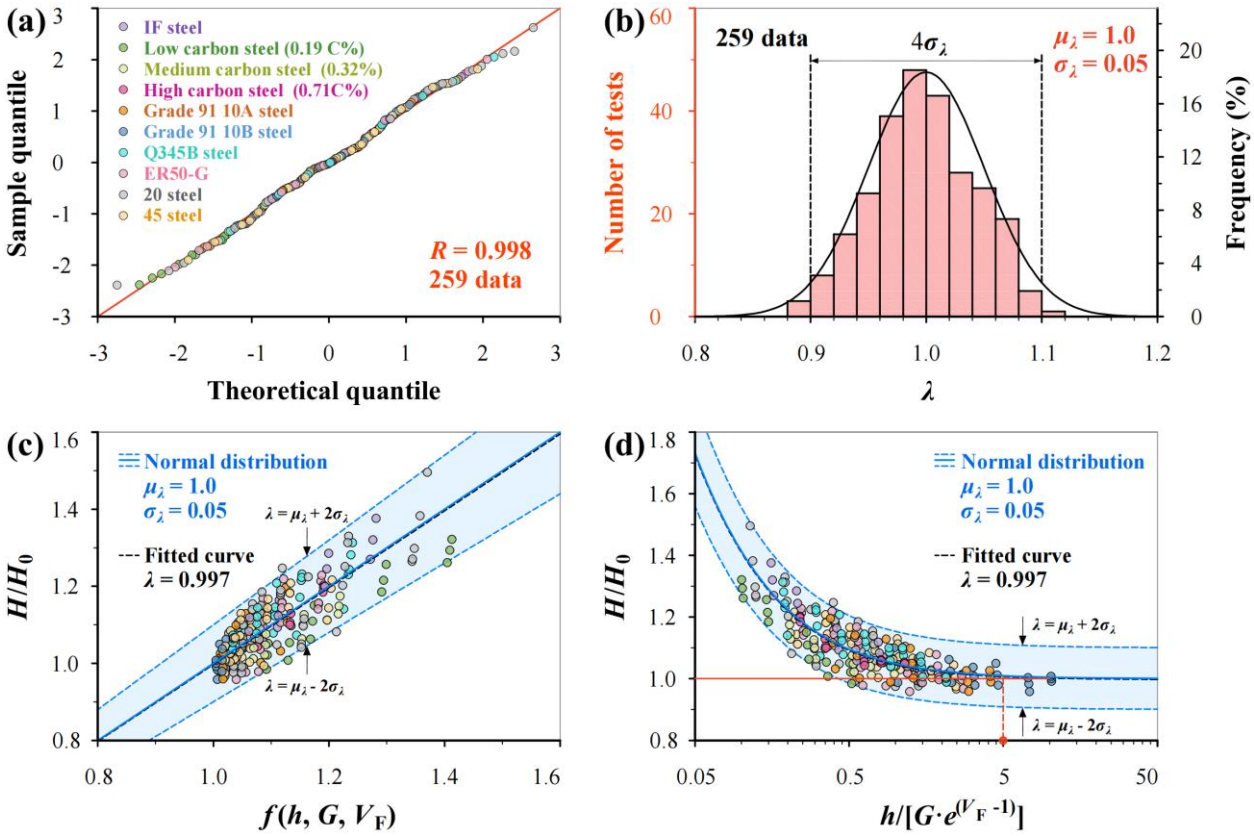

Figure 11. Integrated analysis of hardness measurements on 10 BCC steels. (**a**) q-q plot, (**b**) the histogram of λ values from total of 259 data and normal distribution prediction with μ_λ = 1.0 and σ_λ = 0.05, (**c**) predicted H/H_0–$f(h, G, V_F)$ relations in linearity and (**d**) predicted H/H_0–$h/[G{\cdot}e^{(VF-1)}]$ curves using Equation (19) together with fitted curve and experimental data.

In addition, experimental data exhibiting a non-normal distribution can also be analyzed with Weibull distribution or lognormal distribution. For the application of other statistical models or distribution types, the non-dimensional parameters μ_λ and σ_λ can be modified by adding a skewness coefficient calculated from data.

6. Conclusions

This study investigates microhardness H variation in BCC steels with indentation depth h during micro-indentation hardness tests by analyzing Vickers microhardness

measurements on 10 BCC steels with G from 10.00 μm to 34.41 μm and V_F from 5% to 100%. The main conclusions are as follows:

1. Based on the Nix–Gao model, an analytical relation between H/H_0 and h is proposed, which can replace the fitting method commonly used. Through the proposed model, the hardness of a material H_0 can be calculated based on tested data (h, H) under any loads.
2. The characteristic indentation depth h^* indicates the translation from infinite hardness to macrohardness H_0 in H-h curve. By two methods, h^* is explicitly linked to average grain size G and ferrite volume fraction V_F of BCC steels, i.e., $h^* = 0.1G \cdot e^{(VF-1)}$.
3. In micro-indentation hardness tests, when the indentation depth h is more than $5G \cdot e^{(VF-1)}$, the tested value $H \leq 1.025H_0$ which can be regarded as material hardness H_0.
4. Normal distribution theory is incorporated successfully to quantify the inevitable scatter of hardness measurements resulting from the microstructure heterogeneity of a material and machining/testing errors. After considering scatter, this model includes both mean, and upper and lower bounds with 96% reliability, which ensue effective application for material testing and quality control.

Author Contributions: Conceptualization, A.X.; Methodology, M.Y. and C.Z.; Software, M.Y. and Y.W.; Validation, A.X.; Formal analysis, A.X.; Resources, X.S., M.Y. and Y.W.; Data curation, A.X.; Writing—original draft, A.X.; Writing—review & editing, A.X. and C.Z.; Supervision, X.S. and Y.W.; Funding acquisition, C.Z. All authors have read and agreed to the published version of the manuscript.

Funding: This work was supported by the National Natural Science Foundation of China (52375141, 11672048 and 52105398), the Belt and Road Project (DL2022171003L), Shaanxi Province (2022JM-002) and Chang'an University (300102251302).

Institutional Review Board Statement: Not applicable.

Informed Consent Statement: Not applicable.

Data Availability Statement: The raw data supporting the conclusions of this article will be made available by the authors on request.

Conflicts of Interest: The authors declare no conflict of interest.

Nomenclature

H	Tested hardness or microhardness
H_0	Material hardness or macrohardness
h	Indentation depth
h^*	Characteristic indentation depth as the translation from infinite hardness to H_0
G	Average grain size
V_F	Ferrite volume fraction
b	Burgers vector
μ	Shear modulus
θ	Indenter geometry parameter
f	Scaling factor
σ_y	Yield strength
σ_{GB}	The contribution of grain boundaries to strength
σ_0	The contribution of strengthening other than grain boundaries strengthening.
G_r	Relative grain size
ρ_G	The density of geometrically necessary dislocation
ρ_S	The density of statistically stored dislocation
L	Dislocation mean free path
λ	Non-dimensional parameter
μ_λ	Mean of a group of λ
σ_λ	Standard deviation of a group of λ

References

1. Luo, Q.; Kitchen, M. Microhardness, Indentation Size Effect and Real Hardness of Plastically Deformed Austenitic Hadfield Steel. *Materials* **2023**, *16*, 1117. [CrossRef] [PubMed]
2. Broitman, E. Indentation Hardness Measurements at Macro-, Micro-, and Nanoscale: A Critical Overview. *Tribol. Lett.* **2016**, *65*, 2–18. [CrossRef]
3. Yang, B.; Vehoff, H. Dependence of nanohardness upon indentation size and grain size—A local examination of the interaction between dislocations and grain boundaries. *Acta Mater.* **2007**, *55*, 849–856. [CrossRef]
4. Hu, J.; Sun, W.; Jiang, Z.; Zhang, W.; Lu, J.; Huo, W.; Zhang, Y.; Zhang, P. Indentation size effect on hardness in the body-centered cubic coarse-grained and nanocrystalline tantalum. *Mater. Sci. Eng. A* **2017**, *686*, 19–25. [CrossRef]
5. Bond, T.; Badmos, A.; Ahmed, R.A.; Obayemi, J.D.; Salifu, A.; Rahbar, N.; Soboyejo, W.O. Indentation size effects in aluminum and titanium alloys. *Mater. Sci. Eng. A* **2022**, *839*, 142542. [CrossRef]
6. Mattucci, M.A.; Cherubin, I.; Changizian, P.; Skippon, T.; Daymond, M.R. Indentation size effect, geometrically necessary dislocations and pile-up effects in hardness testing of irradiated nickel. *Acta Mater.* **2021**, *207*, 116702. [CrossRef]
7. Nix, W.D.; Gao, H. Indentation size effects in crystalline materials: A law for strain gradient plasticity. *J. Mech. Phys. Solids* **1998**, *46*, 411–425. [CrossRef]
8. Manika, I.; Maniks, J. Size effects in micro- and nanoscale indentation. *Acta Mater.* **2006**, *54*, 2049–2056. [CrossRef]
9. Jung, B.; Lee, H.; Park, H. Effect of grain size on the indentation hardness for polycrystalline materials by the modified strain gradient theory. *Int. J. Solids Struct.* **2013**, *50*, 2719–2724. [CrossRef]
10. Durst, K.; Backes, B.; Göken, M. Indentation size effect in metallic materials: Correcting for the size of the plastic zone. *Scr. Mater.* **2005**, *52*, 1093–1097. [CrossRef]
11. Qu, S.; Huang, Y.; Pharr, G.M.; Hwang, K.C. The indentation size effect in the spherical indentation of iridium: A study via the conventional theory of mechanism-based strain gradient plasticity. *Int. J. Plast.* **2006**, *22*, 1265–1286. [CrossRef]
12. Sarangi, S.S.; Lavakumar, A.; Singh, P.K.; Katiyar, P.K.; Ray, R.K. Indentation size effect in steels with different carbon contents and microstructures. *Mater. Sci. Technol.* **2022**, *39*, 338–346. [CrossRef]
13. Chicot, D. Hardness length-scale factor to model nano- and micro-indentation size effects. *Mater. Sci. Eng. A* **2009**, *499*, 454–461. [CrossRef]
14. Seekala, H.; Bathini, L.; Wasekar, N.P.; Krishnaswamy, H.; Sudharshan Phani, P. A unified approach to quantify the material and geometrical effects in indentation size effect. *J. Mater. Res.* **2023**, *38*, 1740–1755. [CrossRef]
15. Qin, J.; Huang, Y.; Hwang, K.C.; Song, J.; Pharr, G.M. The effect of indenter angle on the microindentation hardness. *Acta Mater.* **2007**, *55*, 6127–6132. [CrossRef]
16. Shen, F.; Münstermann, S.; Lian, J.A. unified fracture criterion considering stress state dependent transition of failure mechanisms in bcc steels at –196 °C. *Int. J. Plast.* **2022**, *156*, 103365. [CrossRef]
17. Liu, Z.; Yang, L.; Zhang, G.; Zhao, L.; Shao, Q.; Huang, D.; Zhu, Y.; Wang, X.; Shen, Z.; Yang, H. Correlation of microstructure and hardness distribution of high-speed train wheels under original and service statuses. *Eng. Fail. Anal.* **2024**, *158*, 107994. [CrossRef]
18. Mendas, M.; Benayoun, S.; Miloud, M.H.; Zidane, I. Microhardness model based on geometrically necessary dislocations for heterogeneous material. *J. Mater. Res. Technol.* **2021**, *15*, 2792–2801. [CrossRef]
19. Ramazani, A.; Mukherjee, K.; Prahl, U.; Bleck, W. Modelling the effect of microstructural banding on the flow curve behaviour of dual-phase (DP) steels. *Comput. Mater. Sci.* **2012**, *52*, 46–54. [CrossRef]
20. Zhang, C.; Hu, X.; Sercombe, T.; Li, Q.; Wu, Z.; Lu, P. Prediction of ceramic fracture with normal distribution pertinent to grain size. *Acta Mater.* **2018**, *145*, 41–48. [CrossRef]
21. Zhang, C.; Yang, S. Probabilistic prediction of strength and fracture toughness scatters for ceramics using normal distribution. *Materials* **2019**, *12*, 727. [CrossRef] [PubMed]
22. Wang, R.; Gu, H.; Zhu, S.; Li, K.; Wang, J.; Wang, X.; Hideo, M.; Zhang, X.; Tu, S. A data-driven roadmap for creep-fatigue reliability assessment and its implementation in low-pressure turbine disk at elevated temperatures. *Reliab. Eng. Syst. Saf.* **2022**, *225*, 108523. [CrossRef]
23. Gu, H.; Wang, R.; Zhu, S.; Wang, X.; Wang, D.; Zhang, G.; Fan, Z.; Zhang, X.; Tu, S. Machine learning assisted probabilistic creep-fatigue damage assessment. *Int. J. Fatigue* **2022**, *156*, 106677. [CrossRef]
24. *ASTM E92*; Standard Test Methods for Vickers Hardness of Metallic Materials. ASTM International: West Conshohocken, PA, USA, 2018.
25. *ASTM E112*; Standard Test Methods for Determining Average Grain Size. ASTM International: West Conshohocken, PA, USA, 2012.
26. Kobayashi, S.; Sawada, K.; Hara, T.; Kushima, H.; Kimura, K. The formation and dissolution of residual δ ferrite in ASME Grade 91 steel plates. *Mater. Sci. Eng. A* **2014**, *592*, 241–248. [CrossRef]
27. Ragab, M.; Liu, H.; Ahmed, M.M.Z.; Yang, G.; Lou, Z.; Mehboob, G. Microstructure evolution during friction stir welding of 1Cr11Ni2W2MoV martensitic stainless steel at different tool rotation rates. *Mater. Charact.* **2021**, *182*, 11561. [CrossRef]
28. Lavakumar, A.; Sarangi, S.S.; Chilla, V.; Narsimhachary, D.; Ray, R.K. A "new" empirical equation to describe the strain hardening behavior of steels and other metallic materials. *Mater. Sci. Eng. A* **2021**, *802*, 140641. [CrossRef]
29. Siefert, J.A.; Shingledecker, J.P.; Parker, J.D. Optimization of Vickers hardness parameters for micro- and macro-indentation of Grade 91 steel. *J. Test. Eval.* **2013**, *41*, 778–787. [CrossRef]

30. Yaguchi, M.; Tomobe, M.; Komazaki, S.-I.; Kumada, A. Thickness of small sample for creep property evaluation of 9Cr steel base metal of piping on site. *Trans. JSME* **2022**, *88*, 00302. (In Japanese) [CrossRef]
31. Sawada, K.; Kushima, H.; Tabuchi, M.; Kimura, K. Microstructural degradation of Gr.91 steel during creep under low stress. *Mater. Sci. Eng. A* **2011**, *528*, 5511–5518. [CrossRef]
32. Cui, L.; Yu, C.; Jiang, S.; Sun, X.; Peng, R.; Lundgren, J.; Moverare, J. A new approach for determining GND and SSD densities based on indentation size effect: An application to additive-manufactured Hastelloy X. *J. Mater. Sci. Technol.* **2022**, *96*, 295–307. [CrossRef]
33. Iza-Mendia, A.; Gutiérrez, I. Generalization of the existing relations between microstructure and yield stress from ferrite-pearlite to high strength steels. *Mater. Sci. Eng. A* **2013**, *561*, 40–51. [CrossRef]
34. Hall, E.O. The deformation and ageing of mild steel: III Discussion of results. *Proc. Phys. Soc.* **1951**, *64*, 747. [CrossRef]
35. Jiang, L.; Fu, H.; Zhang, H.; Xie, J. Physical mechanism interpretation of polycrystalline metals' yield strength via a data-driven method: A novel Hall-Petch relationship. *Acta Mater.* **2022**, *231*, 117868. [CrossRef]
36. Seok, M.; Choi, I.; Moon, J.; Kim, S.; Ramamurty, U.; Jang, J. Estimation of the Hall-Petch strengthening coefficient of steels through nanoindentation. *Scr. Mater.* **2014**, *87*, 49–52. [CrossRef]
37. Tabor, D. The hardness and strength of metals. *J. Inst. Met.* **1951**, *79*, 1–18.
38. Hernot, X.; Moussa, C.; Bartier, O. Study of the concept of representative strain and constraint factor introduced by Vickers indentation. *Mech. Mater.* **2014**, *68*, 1–14. [CrossRef]
39. Gutierrez, I. AME modelling the mechanical behaviour of steels with mixed microstructures. *J. Metall. Mater. Eng.* **2005**, *11*, 201–214.